Article ID: 1000-5773(2006)02-0194-08

Single-Domain Nanosphere Observation and Ferromagnetic/Antiferromagnetic Coupling of Ni/NiO*

LIU Xian-Song[1], ZHANG Cheng-Wen[1], ZHOU Sheng-Qiang[1], YIN Ping[1], Udi Meridor[2], Aviad Frydman[2], Aharon Gedanken[3]

(1. *Anhui Key Laboratory of Information Materials & Devices, School of Physics & Materials Science, Anhui University, Hefei* 230093, *China*;
2. *The Physics Department and the Minerva Center, Bar-Ilan University, Ramat Gan* 52900, *Israel*;
3. *Department of Chemistry, Bar-Ilan University, Ramat-Gan* 52900, *Israel*)

Abstract: Magnetic force microscopy (MFM) measurements were performed on monodispersed single-domain nickel nanospheres fabricated by the microwave-assisted (MW) polyol method. As found by MFM, a relevant characteristic of these spheres with a size distribution in the 100～180 nm range is the magnetic stripe domain structure. The obtained highly globular nanostructures of $Ni_{core}NiO_{shell}$ were measured by XRD, TEM, XPS, and EDAX. The ferromagnet/antiferromagnet interface coupling is discussed with the results of VSM and SQUID. The relation of the exchange-coupling field with particles sizes is evaluated.

Key words: monodispersed single-domain nickel nanospheres; $Ni_{core}NiO_{shell}$; ferromagnet/antiferromagnet interface coupling

CLC number: O482.52 **Document code**: A

1 Introduction

The synthesis and characterization of nanostructured materials is aimed at designing and arranging nanomaterials in complex functional structures, resulting in unique physical properties[1-6]. Metal magnetic nanoparticles, especially those having a spherical core-shell structure, have received a considerable amount of attention in recent years[7-10]. This is due to the structure-property relations that have led to important applications, such as materials for ultrahigh-density data storage, magnetic nanodevices, and medicine[11-16]. Nickel has been used for wide applications in areas such as catalysis, fuel cell electrodes, and magnetic storage media[17-21]. The methods by which nickel nanoparticles were fabricated are: ultrasound irradiation[22], chemical reduction[23], evaporation technique[24], and the polyol method[25].

In the current study, the microwave-assisted (MW) polyol method is used to obtain monodispersed nickel spheres with diameters ranging from 100～180 nm. Although the conventional polyol method was previously used to prepare submicron metallic nickel particles, the corresponding reaction under MW radiation has never been reported. Furthermore, in this work we report on the formation of core-shell structures of highly globular $Ni_{core}NiO_{shell}$, which are synthesized from the Ni spheres, and

* **Received date**: 2004-11-18; **Revised date**: 2005-01-13

Foundation Item: This research is supported by an European Community grant for the NANOBAT(Project No. NNE5-2001-00042) and the Key Program of the Education Department of Anhui Province under Grant No. 2005KJ033ZD.

Biography: LIU Xian-Song(1962—), male, phD, professor. E-mail: xiansongliu@yahoo.com.cn

the magnetic properties of the core-shell structures are investigated. We should also mention that, unlike the conventional reaction where ethylene glycol was employed as the polyol solvent, in the MW-assisted polyol reaction triethylene glycol (TREG) was used as the solvent.

In the current process, the metallic salt was dissolved in TREG and the product, glycol-metal salt mixture, was then heated by microwave irradiation. Our modified MW oven included a distillation system, and the reaction mixture was refluxed while the metallic moieties precipitated out of the solution. The solution was refluxed at 287 ℃, the b. p. of TREG, which is higher than that of ethylene glycol (196 ℃) used in the conventional polyol reaction.

2 Experimental Section

2.1 Preparation

A two-step approach had been employed in this investigation for the preparation of nickel-nickel oxide. In the first, the starting material was a solution of nickel (Ⅱ) acetate tetrahydrate(99.998%, Aldrich Chemical Co.) in TREG (triethylene glycol) (>99%, Bio Lab Ltd.). Following the previously described process[26], a 100 mL glass flask was placed in a microwave oven (Spectra 900W) and connected to a condenser. Before the reaction, 50 mL of a solution of 0.125 M $Ni(Ac)_2$ in TREG was purged by argon for 20 min, after which the microwave oven was turned on at a power level of 70% with a continued flow of the gas. The reaction was stopped as soon as a black suspension appeared, which was immediately cooled in iced water. The resulting solid product was washed thoroughly with ethanol and centrifuged. All these processes were repeated five times. The nickel spheres product was dried under vacuum and kept in a glove box.

In the second synthetic step, 100 mg of nickel spheres, put in a porcelain boat, was introduced into a tubular furnace. During the reaction, oxygen at a flow rate of 100 cm^3/min was bubbled through a solution of hydrogen peroxide (H_2O_2 of 30%, Bio Lab Ltd.). The reaction took 3 h at different temperatures: 300, 325, 350 ℃. At the end of the reaction, the cell was cooled down with continued purging of the gas.

2.2 Characterization

The powder X-ray diffraction (XRD) patterns were collected on a Bruker AXS D* Advance Powder X-ray diffractometer (using Cu-K_α radiation $\lambda = 0.15418$ nm). The particle size, morphology, and nature of the NiO/Ni particles were studied by transmission electron microscopy (TEM) employing a JEOL-JEM 100 SX microscope working at 100 kV. Samples for the TEM experiments were prepared by suspending the dried sample in absolute ethanol in a sonication bath for 20 min. In order to examine the dimensions and mechanical stability of the nanospheres, we employed a Digital Instruments 3100 dimension AFM. For the AFM measurements the particles were spin coated on a Si substrate and were scanned in the tapping mode. The AFM(Atomic Force Microscopy) tips used for the scan were TAP300 tips made by NanoDevices and TAP300 made by BudgetSensors. We used an MFM(Magnetic Force Microscopy) tip and scanned the particles, once for their topography and then 40 nm above their surface in order to study the magnetization, and to observe whether the particles are single domain. The MFM tips used for the scanning process were MESP Veeco nanoprobe tips. X-ray photoelectron spectroscopy (XPS) was recorded using an AXIS, HIS 165, ULTRA (Kratos Analytical). The Ar^+ sputtering was carried out for 15 min at an energy of 4 keV and a current density of 0.5 $\mu A/cm^2$. Under these conditions the estimated surface removal depth was 1.0～1.5 nm. The elemental composition of the material was analyzed by energy-dispersive X-ray analysis (EDAX; JEOL-JSM 840 scanning electron microscope).

Magnetic measurements at room temperature were conducted using an Oxford Instrument vibrating sample magnetometer (VSM). 20～25 mg of nickel nanoparticles were inserted into the gelatin capsule and plugged with cotton to prevent dispersal of the powder. Temperature-resolved magnetic measurements were conducted using a Quantum Design MPMS SQUID magnetometer. Specifically, measurements were performed by cooling a sample in zero field down to 4 K, when a magnetic field of 1.59 MA/m was applied. After that, the sample was slowly warmed up to a high temperature (typically 300 K) in steps of a few K per minute with stabilization at each temperature level and subsequent measurement of the magnetic moment (ZFC). Then, without turning the field off, the sample was cooled down to 4 K while measuring the magnetic moment at each intermediate temperature (FC). To induce the maximal unidirectional anisotropy at Ni/NiO interface, a magnetic field (0.80 MA/m) should be applied during cooling at 550 K to 300 K by using the above-mentioned VSM. Then, the sample was moved to the SQUID hood and cooled down to 4 K with a magnetic field of 1.59 MA/m while measuring the magnetic moment (FC) at the corresponding temperature point of ZFC.

3 Results and Discussion

3.1 Characterization and Morphology

Fig. 1(a) presents the XRD patterns of the precipitated powder. The position of the diffraction peaks matches closely the reported JCPDS (4-850) data. The product is therefore identified as FCC crystalline nickel.

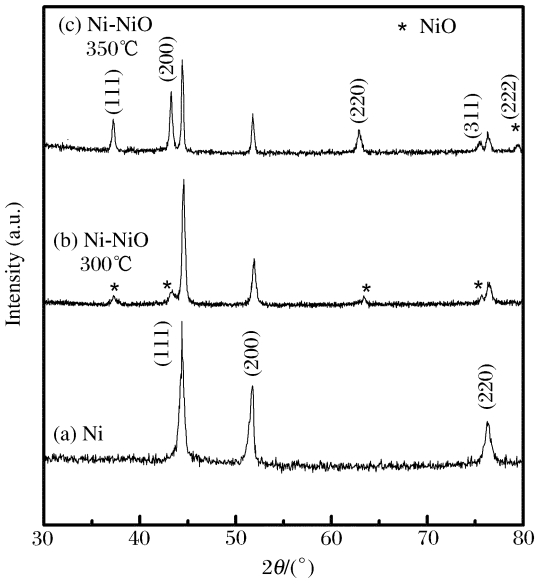


Fig. 1 X-ray powder diffraction pattern of the samples

Fig. 2(a) presents a magnified TEM image of a single ～180 nm nickel sphere before it undergoes oxidation by H_2O_2. Fig. 2(b), which depicts a number of Ni spheres after oxidation, shows the existence of an outer shell having a brighter image than the dark inner core. In addition, we detect some small particles on the surface of the globular Ni. This also confirms the formation of the nickel-nickel oxide core-shell structure. The core-shell nanosphere particles (Fig. 2(b)) have a morphology similar to that of the nickel balls (Fig. 2(a)), and the NiO-extended Ni sphere particles have a uniform and remarkably thin NiO layer with 30 nm of the shell thickness on their outer surface.

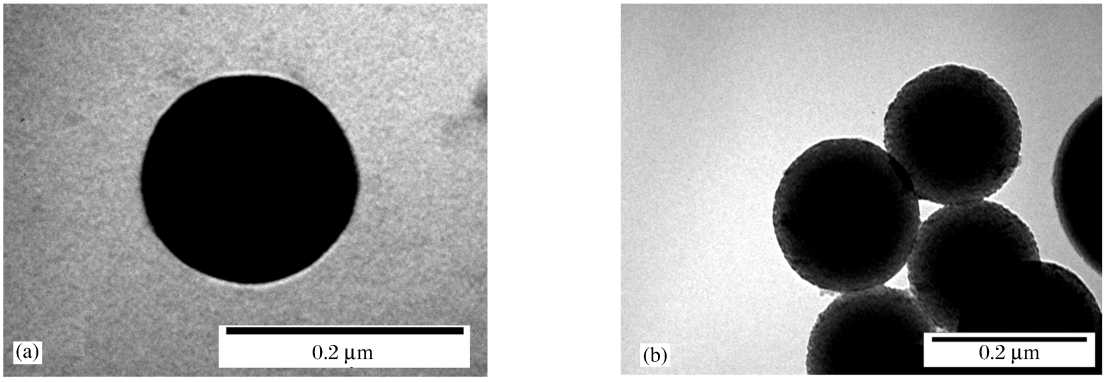


Fig. 2 TEM of (a) a nickel sphere, (b) highly spherical $Ni_{core}NiO_{shell}$ nanostructures

The thickness of the NiO outer layer depends on the reaction time, the reaction temperature, and the amount of H_2O_2 flowing through the solution. In an attempt to control the thickness of the NiO layer, we have varied the reaction temperature while keeping all other parameters constant. The reaction time was fixed at 3 h and the flow rate of H_2O_2 at 100 cm^3/min. As could be expected, we have found that as the reaction temperature increased, a thicker NiO shell was obtained. A NiO shell thickness of about 30 nm was obtained for a reaction temperature of 350 ℃ (Fig. 2(b)). Simultaneously, we observed an increase in the intensity of the XRD diffraction peaks of nickel oxide (Fig. 1(b) and Fig. 1(c)) and a smooth uniform NiO shell was observed for all oxidation temperatures.

The morphological studies were performed by AFM measurements. Fig. 3 shows a typical AFM micrograph of Ni spheres, demonstrating that the average size of the particles is below 180 nm in diameter and 180 nm in height. In order to test their mechanical stability, we tried to move them using AFM manipulation in a non-contact mode. The spheres maintained their original geometry without a noticeable change in their overall shape. The picture shown in Fig. 3 is representative of a large number of nanospherical particles that have been scanned and measured by the AFM and MFM techniques.

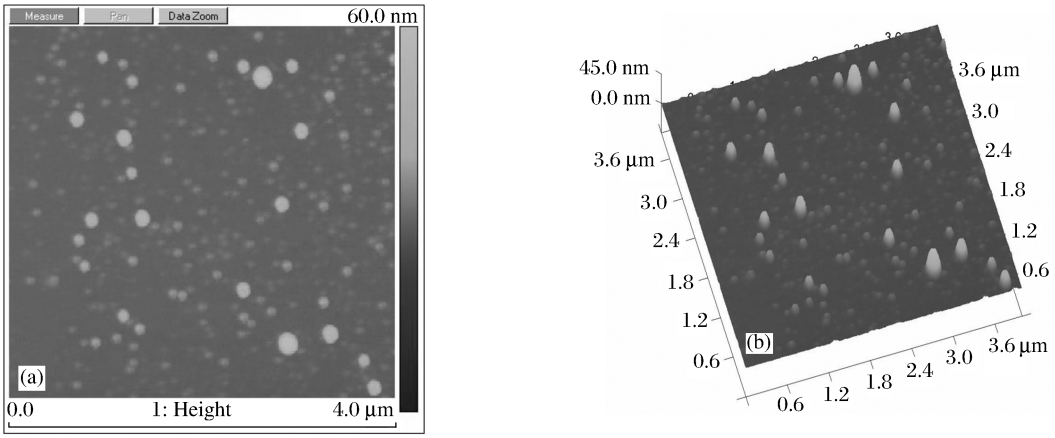


Fig. 3　2D(a) and 3D(b) AFM images of monodisperse nickel nanospheres
(The hights metioned in the text were taken from the 2D image)

Fig. 4 shows four scans of MFM images of two types of particles. The first is an image of an individual particle, while the second is a picture of two connected nanospheres. Each pair of AFM and MFM images was measured in the same region. Fig. 4(b) illustrates that the orientation of the magnetization is identical for the whole particle, or, in other words, the 100～180 nm nickel particles are single-domain structures. Fig. 4(c) shows two magnetic nanospherical particles. However, for the two-connected Ni spheres we can distinctly observe two domain structures possessing different magnetization regions.

The surface of the core-shell structure of the as-prepared samples was also characterized by X-ray photoelectron spectroscopy (XPS). The binding energy of the $2p_{3/2}$ core electron, is 854.4 eV (Fig. 5), which is in good agreement with the XPS data of Ni^{2+} ions. The position of the Ni^0 $2p_{3/2}$ peak is expected at 853.0 eV. The O(1*s*) XPS spectrum (Insert of Fig. 5) reveals a very broad signal at around 529.0 eV. The 529.0 eV O(1*s*) peak is attributed to the oxygen atom bonded to the divalent nickel. The XPS spectrum shows the presence of Ni^{2+} and oxygen on the outer layer of the globular particles, with atomic concentrations of 44.5% and 55.5%, respectively. The stoichiometric ratio found from the area under the XPS peak indicates a slight excess of oxygen, which we attribute to water molecules adsorbed on the surface of the particles[27].

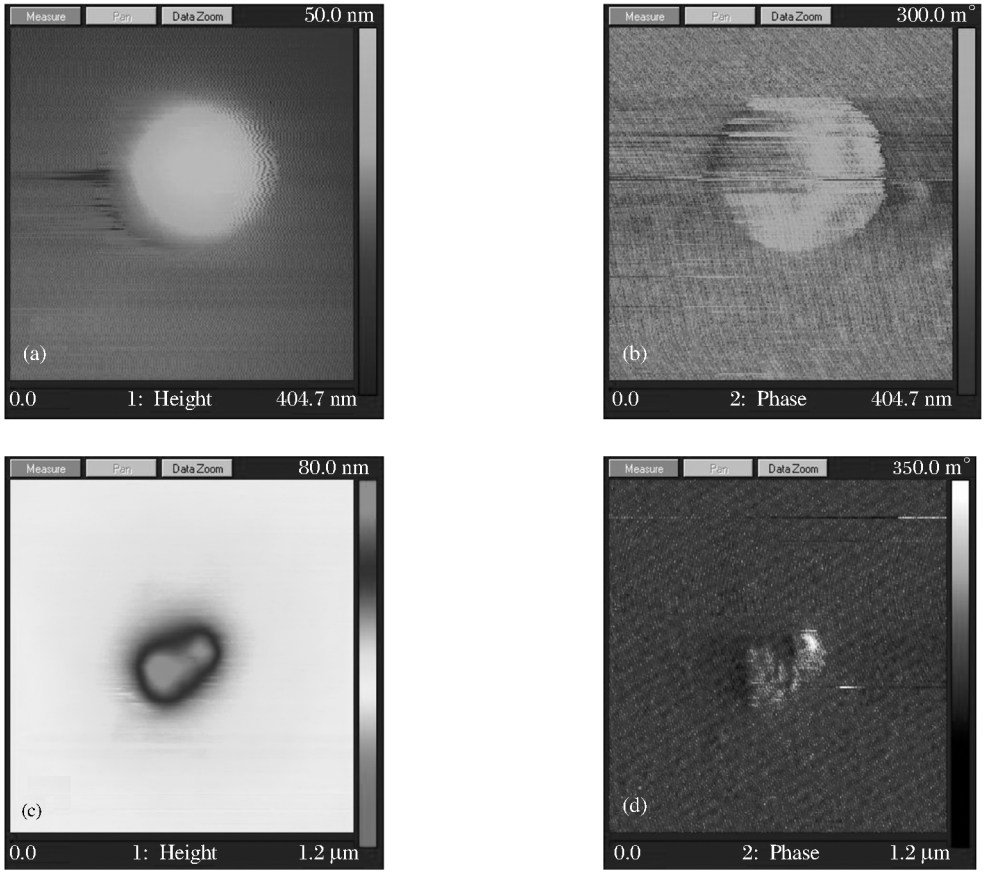


Fig. 4 Magnetic domain structure of monodisperse nickel nanospheres observed using an MFM ((a) A topographic scan by AFM for one sphere, (b) MFM image of the particle of Fig. 4(a) showing one domain structure, (c) AFM image of two-connected nanospheres, (d) MFM image of Fig. 4(c) demonstrating two magnetic domains)

The elemental composition of the core-shell spheres was also analyzed by EDAX. A quantitative measurement of the nickel spheres before and after oxidation was 92.94% and 57.80% (atomic percent), respectively. Although it is well known that EDAX is not a good quantitative method for light elements such as oxygen, the numbers obtained, 7.06% and 42.20%, show the expected trend of the successful oxidation of the particle's surface.

3.2 Magnetic Properties

The results of the room temperature hysteresis loop measured by VSM under an applied magnetic field of 1.6 T, are depicted in Fig. 6. Typical ferromagnetic properties of the Ni nanospheres are observed, of which the saturation magnetization M_S and coercivity H_C are 44 emu/g and 3.18 kA/m, respectively.

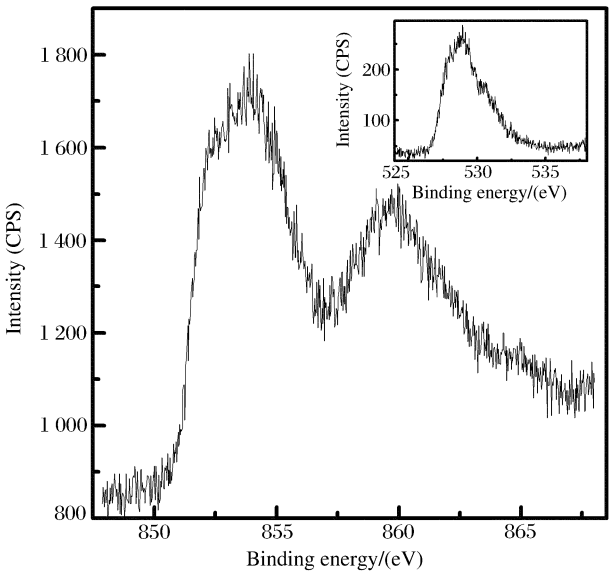


Fig. 5 XPS-spectra of $Ni_{core}NiO_{shell}$ spheres for nickel particles oxidized at 300 ℃ (Inset is the O 1*s* XPS spectrum)

Note that the curve is symmetric around $H=0$.

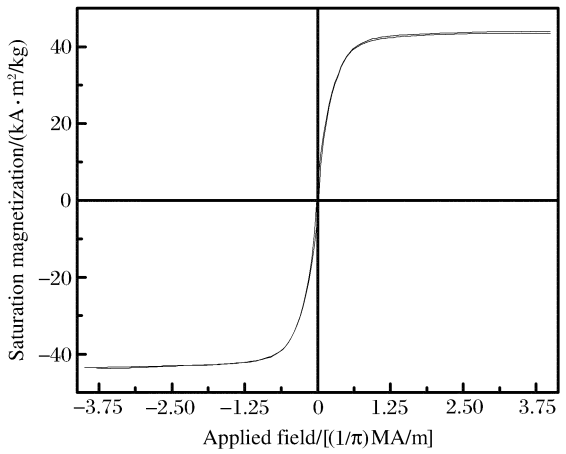


Fig. 6　Hysteresis loop of the nickel nanospheres measured by VSM at room temperature

Exchange bias is one of the phenomena associated with the exchange anisotropy created at the interface between an AFMG (antiferromagnetic) and FM (ferromagnetic) materials. It occurs in a large variety of systems which are composed of an AFMG in atomic contact with a FM if the sample is grown, or after the system is cooled, below the respective Néel and Curie temperatures, T_N and T_C, in an external cooling field H[28-29]. The main manifestation of this effect is a shift in the M-H loop so that the magnetization curve is not symmetric around $H=0$. This result is expected in our spheres since we have Ni (FM) cores surrounded by NiO (AFMG).

Magnetization measurements as a function of temperature were performed by zero-field-cooling (ZFC) and field-cooling (FC) procedures at an applied magnetic field ($H=1.59$ MA/m). M_{ZFC} was measured while warming from 4 to 300 K, whereas M_{FC} was recorded during the subsequent cooling. Before M_{FC} was recorded during the subsequent cooling, a magnetic field (0.80 MA/m) should be applied during cooling from 550 K to 300 K under VSM and 1.59 MA/m is used from 300 K to 4 K in SQUID. Fig. 7 compares the ZFC and FC loops, showing no sign of the exchange bias effect. The M-H loops are symmetric, showing no sign of a shift. Both ZFC and FC magnetization curves rapidly decrease with the increase of temperature and reveal no intersection in the whole range shown in Inset (b) of Fig. 7. In this respect our particles, for which the ZFC magnetization curve coincides with the FC magnetization, are similar to the system of 20 nm iron particles embedded in PMMA[30]. This is in contrast to other literature reports relating to Ni/NiO particles with an average particle size below 30 nm, which have demonstrated a nonsymmetrical magnetic hysteresis loop[31-32].

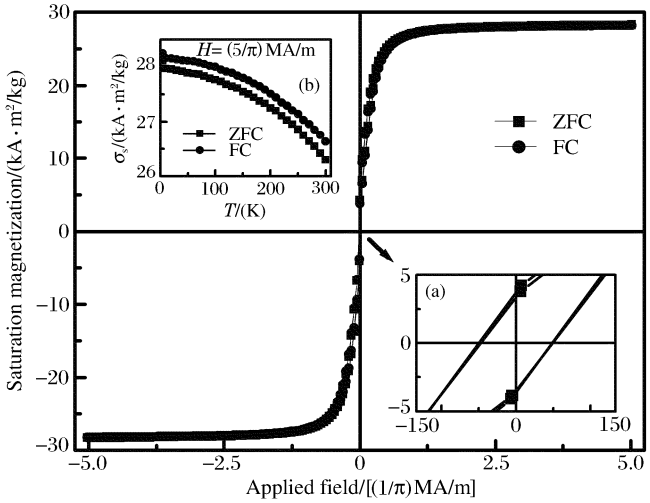


Fig. 7　Hysteresis loops at 4 K of $Ni_{core}NiO_{shell}$ sphere particles (Note that the results for FC and ZFC are practically indistinguishableand in both cases no shift is observed)
Inset: (a) A zoom of the curve near the origin point for ZFC and FC. Note the symmetry around $H=0$.
(b) ZFC and FC magnetization curves as a function of temperature from 4～300 K

When FM-AFMG structures are prepared to give a large exchange bias, one normally cools the material in a magnetic field from a temperature above the Néel temperature (above 500 K) of the AFMG. It is important for us to observe nonsymmetrical hysteresis loop although our measurement did like many published papers[24,33]. So it can be understood by assuming that H_{ex} (an exchange field)

is formally equivalent to an external field, the coupling energy difference between two FM moment directions[11] is given by

$$\Delta E = -\frac{1}{2}\Delta\chi_{\mathrm{AFGM}}\mu_0 H_{\mathrm{ex}}^2 \tag{1}$$

where $\Delta\chi_{\mathrm{AFMG}}$ is the associated difference in susceptibility of the interface AFMG. The minimum energy of $Ni_{core}NiO_{shell}$ particles for coherent rotation of the FM moments is

$$\Delta E_{\min} = \mu_0 H_c M_s V_{\mathrm{FM}} \tag{2}$$

where VFM is the FM Ni core volume and M_S is the saturation magnetization. Since the spherical volume is proportional to r^3 (the spherical radius), one can expect a significant difference in H_{ex} between our particles (of about 180 nm $Ni_{core}NiO_{shell}$ spheres) and previously reported particles (below 30 nm). In addition, it should be noted that for the small particles[34-36], the thickness of the AFMG and FM are of the same order, and hence the effect of the AFMG can be expected to be much larger.

4 Conclusions

We have presented a new method of fabricating monodispersed nickel spheres and highly globular nanostructures of $Ni_{core}NiO_{shell}$. These monodispersed nickel spheres, in a size range below 180 nm, are characterized by a magnetic single domain structure. The present results demonstrate that the magnetic coupling in a $Ni_{core}NiO_{shell}$ structure induces an anisotropy that is not enough to cause a shift in the *M-H* loop due to the large FM core volume. Such spherical particles could be very helpful in the study of magnetically-ordered structures and are expected to provide insight into the understanding of exchange-coupling anisotropy in core-shell particle structures.

References:

[1] Caruso F, Caruso R A, Möhwald H. Nanoengineering of Inorganic and Hybrid Hollow Spheres by Colloidal Templating [J]. Science, 1998, 282: 1111-1114.

[2] Hall S R, Davis S A, Mann S. Co-Condensation of Organosilica Hybrid Shells on Nanoparticle Templates: A Direct Synthetic Route to Functionalized Core-Shell Colloids [J]. Langmuir, 2000, 16: 1454-1456.

[3] Karmhag R, Niklasson G A, Nygren M. Oxidation Kinetics of Nickel Nanoparticles [J]. J Appl Phys, 2001, 89: 3012-3017.

[4] Jang J, Lim B. Facile Fabrication of Inorganic-Polymer Core-Shell Nanostructures by a One-Step Vapor Deposition Polymerization [J]. Angew Chem Int Ed, 2003, 42: 5600-5603.

[5] Teng X W, Yang H. Synthesis of Face-Centered Tetragonal FePt Nanoparticles and Granular Films from Pt@Fe_2O_3 Core-Shell Nanoparticles [J]. J Am Chem Soc, 2003, 125: 14559-14563.

[6] Caruso F, Susha A S, Giersig M, et al. Magnetic Core-Shell Particles: Preparation of Magnetite Multilayers on Polymer Latex Microspheres [J]. Adv Mater, 1999, 11: 950-953.

[7] Vestal C R, Zhang Z J. Atom Transfer Radical Polymerization Synthesis and Magnetic Characterization of MnFe_2O_4/Polystyrene Core/Shell Nanoparticles [J]. J Am Chem Soc, 2002, 124: 14312-14313.

[8] Park J I, Cheon J. Synthesis of 'Solid Solution' and 'Core-Shell' Type Cobalt-Platinum Magnetic Nanoparticles via Transmetalation Reactions [J]. J Am Chem Soc, 2001, 123: 5743-5746.

[9] Sobal N S, Ebels U, Mohwald H. Synthesis of Core-Shell PtCo Nanocrystals [J]. J Phys Chem B, 2003, 107: 7351-7354.

[10] Lyon J L, Fleming D A, Stone M B, et al. Synthesis of Fe Oxide Core/Au Shell Nanoparticles by Iterative Hydroxylamine Seeding Source [J]. Nano Lett, 2004, 4(4): 719-723.

[11] Skumryev V, Stoyanov S, Zhang Y, et al. Beating the Superparamagnetic Limit with Exchange Bias [J]. Nature, 2003, 423: 850-853.

[12] Eisenmenger J, Schuller I V. Overcoming Thermal Fluctuations [J]. Nat Mater, 2003, 2: 437-438.

[13] Sun S H, Murray C B, Weller D, et al. Monodisperse FePt Nanoparticles and Ferromagnetic FePt Nanocrystal Superlattices [J]. Science, 2000, 287: 1989-1992.

[14] Kodama R H. Magnetic Nanoparticles [J]. J Magn Magn Mater, 1999, 200: 359-372.

[15] Lubbe A S, Alexiou C, Bergemann C. Clinical Applications of Magnetic Drug Targeting [J]. J Surg Res, 2001, 95: 200-2006.

[16] Tu Y, Huang Z P, Wang D Z, et al. Growth of Aligned Carbon Nanotubes with Controlled Site Density [J]. Appl Phys Lett, 2002, 80: 4018-4020.

[17] Zhang P,Zuo F,Urban F K,et al. Irreversible Magnetization in Nickel Nanoparticles [J]. J Magn Magn Mater,2001,225:337-345.
[18] Lok J G S,Geim A K,Maan J C. Memory Effects in Individual Submicrometer Ferromagnets [J]. Phys Rev B,1998,58:12201-12206.
[19] Cordente N,Amiens C B,Chaudret B,et al. Chemisorption on Nickel Nanoparticles of Various Shapes:Influence on Magnetism [J]. J Appl Phys,2003,94:6358-6365.
[20] Zhou H,Kumar D,Kvit A,et al. Formation of Self-Assembled Epitaxial Nickel Nanostructures [J]. J Appl Phys,2003,94:4841-4846.
[21] Meiklejohn H,Bean C P. New Magnetic Anisotropy [J]. Phys Rew,1956,102:1413-1414.
[22] Palchik O,Kataby G,Mastai Y,et al. New Method for Nanofabrication of Structures Analogous to 'Core-Shell' Vesicles [J]. Adv Mater,1999,11:1289-1292.
[23] Ross C A,Farhoud M,Hwang M,et al. Micromagnetic Behavior of Conical Ferromagnetic Particles [J]. J Appl Phys,2001,89:1310- 1319.
[24] Yao Y D,Chen Y Y,Tai M F,et al. Magnetic Anisotropy Effects in Nano-Cluster Nickel Particles [J]. Mat Sci Eng A,1996,217:281- 285.
[25] Vaidhyanathan B,Rao K J. Microwave Assisted Carbothermal Reduction and Nitridation [J]. Chem Mater,1997,9:1196-1198.
[26] Palchik O,Avivi S,Pinkert D,et al. Preparation and Characterization of Ni/NiO Composite Using Microwave Irradiation and Sonication [J]. Nanostruct Mater,1999,11:415-419.
[27] Palchik O,Zhu J J,Gedanken A. Microwave Assisted Preparation of Binary Oxides Nanoparticles [J]. J Mater Chem,2000,10:1251-1255.
[28] Nogués J,Schuller I K. Exchange Bias [J]. J Magn Magn Mater,1999,192:203-232.
[29] Kiwi M. Exchange Bias Theory [J]. J Magn Magn Mater,2001,234:584-595.
[30] Wilson J L,Poddar P,Frey N A,et al. Synthesis and Magnetic Properties of Polymer Nanocomposites with Embedded Iron Nanoparticles [J]. J Appl Phys,2004,95:1439-1443.
[31] Löffler J,Swygenhoven H V,Wagner W,et al. Influence of Grain Size and Oxidation on the Magnetic Properties of Nanostructured Fe and Ni [J]. Nanostruct Mater,1997,9:523- 526.
[32] Löffler J,Wagner W,VanSwygenhoven H,et al. Nanoscale Characterization of Magnetic Properties in Nanostructured Fe,Ni and Co by Small-Angle Neutron Scattering [J]. Nanostruct Mater,1997,9:331-334.
[33] Yao Y D,Chen Y Y,Hsu C M,et al. Thermal and Magnetic Studies of Nanocrystalline Ni [J]. Nanostruct Mater,1995,6:933-936.
[34] Kodama R H,Makhlouf S A,Berkowitz A E. Finite Size Effects in Antiferromagnetic NiO Nanoparticles [J]. Phys Rev Lett,1997,79:1393-1396.
[35] Rusponi S,Cren T,Weiss N,et al. The remarkable Difference Between Surface and Step Atoms in the Magnetic Anisotropy of Two-Dimensional Nanostructures [J]. Nat Mater,2003,2:546-561.
[36] Finazzi M,Portalupi M,Brambilla A,et al. Magnetic Anisotropy of NiO Epitaxial Thin Films on Fe(001) [J]. Phys Rev B,2004,69:014410.

单畴 Ni 球观测及 $Ni_{core}NiO_{shell}$ 的铁磁/反铁磁耦合研究

刘先松[1],章成文[1],周圣强[1],尹　萍[1],Udi Meridor[2],
Aviad Frydman[2],Aharon Gedanken[3]

(1. 安徽省信息材料与器件重点实验室,安徽大学物理与材料学院,安徽合肥　230039;
2. The Physics Department and the Minerva Center,Bar-Ilan University,Ramat Gan 52900,Israel;
3. Department of Chemistry,Bar-Ilan University,Ramat-Gan 52900,Israel)

摘要:使用微波辅助聚合方法制备了单分散单畴 Ni 纳米球,由 MFM 发现,尺度分布在 100～180 nm 的 Ni 球的一个相关特征是条型磁畴结构。用 XRD、TEM、XPS 以及 EDAX 测量了由 Ni 球进一步制备的 $Ni_{core}NiO_{shell}$ 高度球型纳米结构。用 VSM 和 SQUID 进一步讨论了其铁磁/反铁磁界面耦合效应,估算了交换耦合场与粒子尺寸的关系。

关键词:单分散单畴 Ni 纳米颗粒 ;$Ni_{core}NiO_{shell}$ 结构 ;铁磁/反铁磁界面耦合
中图分类号:O482.52　　**文献标识码**:A